Length-scale Effects in Cascade Damage Production in Iron

R. E. Stoller[1], P. J. Kamenski[2], and Yu. N. Osetsky[1]

[1]*Materials Science and Technology Division*
Oak Ridge National Laboratory, Oak Ridge, TN 37831-6138
[2]*Department of Materials Science and Engineering*
University of Wisconsin, Madison, WI
(now University of Oxford, UK)

Abstract

Molecular dynamics simulations provide an atomistic description of the processes that control primary radiation damage formation in atomic displacement cascades. An extensive database of simulations describing cascade damage production in single crystal iron has been compiled using a modified version of the interatomic potential developed by Finnis and Sinclair. This same potential has been used to investigate primary damage formation in nanocrystalline iron in order to have a direct comparison with the single crystal results. A statistically significant number of simulations were carried out at cascade energies of 10 keV and 20 keV and temperatures of 100 and 600K to make this comparison. The results demonstrate a significant influence of nearby grain boundaries as a sink for mobile defects during the cascade cooling phase. This alters the residual primary damage that survives the cascade event. Compared to single crystal, substantially fewer interstitials survive in the nanograined iron, while the number of surviving vacancies is similar or slightly greater than the single crystal result. The fraction of the surviving interstitials contained in clusters is also reduced. The asymmetry in the survival of the two types of point defects is likely to alter damage accumulation at longer times.

Introduction

Primary damage formation in irradiated metals due to atomic displacement cascades has been extensively investigated using the method of molecular dynamics (MD) [1-11]. These MD simulations have led to a well-accepted understanding of the underlying processes that lead to the formation of stable (on MD time scales) distributions of point defects, i.e. vacancies and interstitials. Both types of point defects are found in the form of isolated mono-defects as well as small defect clusters. The influence of variables such as cascade (or primary knock-on atom, PKA) energy and irradiation temperature have been determined [8] and differences due to the choice of interatomic potential have been explored [10]. A particularly large database of simulations has been accumulated for iron [9] using a modified version of the interatomic potential developed by Finnis and Sinclair [3,12]. Like most MD studies of displacement cascades, the simulations in this database were carried out using perfect crystals with periodic boundary conditions. To the extent that the simulations are representative of radiation damage in iron, they represent only the behavior of single crystal materials.

There has been a limited amount of research carried out to investigate the potential influence of grain size on primary damage formation [11, 13-16]. Computational limitations dictate that such work would focus on nanometer grain sizes, and quite strong effects have been

observed [11]. However, there has been no systematic study that statistically demonstrated how a nanograin structure would alter primary damage formation. The same Finnis-Sinclair potential mentioned above has been used in such an investigation of nanocrystalline iron in order to have a direct comparison with the corresponding single crystal database. A sufficient number of simulations were carried out at cascade energies of 10 keV and 20 keV and temperatures of 100 and 600K to obtain a statistically significant comparison. The results demonstrate that the creation of primary radiation damage can be substantially different in nanograined material due to the influence of nearby grain boundaries.

Simulation Method

The simulations were carried out using both serial and parallel versions of the MOLDY [17] MD code and the interatomic potential for iron developed by Finnis and Sinclair [12]. The potential was modified for use in high-energy simulations by Calder and Bacon [3]. This code and potential have been widely used, and the results of the single crystal iron simulations are discussed elsewhere [3,6-9]. All simulations were carried out at constant pressure with periodic boundary conditions. Since the boundary atoms were not damped to remove heat, the kinetic energy of the PKA leads to some lattice heating. This heating has little or no impact on the ballistic phase of the cascade, and the extent to which it may influence the number and configuration of final, stable displacements is not yet clear [8, 18, 19]. Typical MD simulation times are about 15 ps for 10 and 20 keV simulations, which is the time required to dissipate the initial recoil energy and re-thermalize atomic motion. At this point, the number of stable point defects is counted and their configuration determined. The number of isolated point defects (single interstitials and vacancies) and the number of point defects in clusters are determined as well as the size distributions of vacancy and interstitial clusters.

Nanocrystalline construction

To create the nanocrystalline structure, nucleation sites were chosen, the grains were filled using a Voronoi technique [20], overlapping atoms at the grain boundaries were removed, and finally the structure was equilibrated using MD. The nucleation sites were obtained by melting a face centered cubic (fcc) material through Monte Carlo simulation using a simple Lennard-Jones interatomic potential and then scaling the distance between the sites to achieve the desired grain size. This methodology was used over simple random number generation in order to better reproduce a grain size distribution consistent with experiments. A 2x2x2 unit cell system was used resulting in 32 nucleation sites, and hence 32 grains in the final sample.

Each Voronoi polyhedron was filled with atoms placed on a regular bcc iron crystalline lattice, with the lattice orientation randomly selected. Grain boundaries occur naturally when the atomic plains in adjacent polyhedra impinge on one another. Within the boundary region, one atom from any pair of atoms closer than 80% of the nearest neighbor bond distance was removed. This was done to counteract the unphysical situation wherein the Voronoi technique allows atoms in the grain boundary to be arbitrarily close to one another. It should be noted that the exact cutoff distance is unimportant considering there are no volume constraints in the equilibration. In this case, the interatomic potential will dictate the grain boundary density for the given pressure. The final system was periodic and had an average grain size of 10 nm, system

box length of 28.3 nm, and contained roughly 1.87 million atoms. The system was equilibrated for over 200 ps including a heat treatment up to 600 K. Fig. 1 illustrates a typical grain structure with each grain shown in a different color. The approximate sizes of 5 and 20 keV cascades have been projected on to the face of the simulation cell.

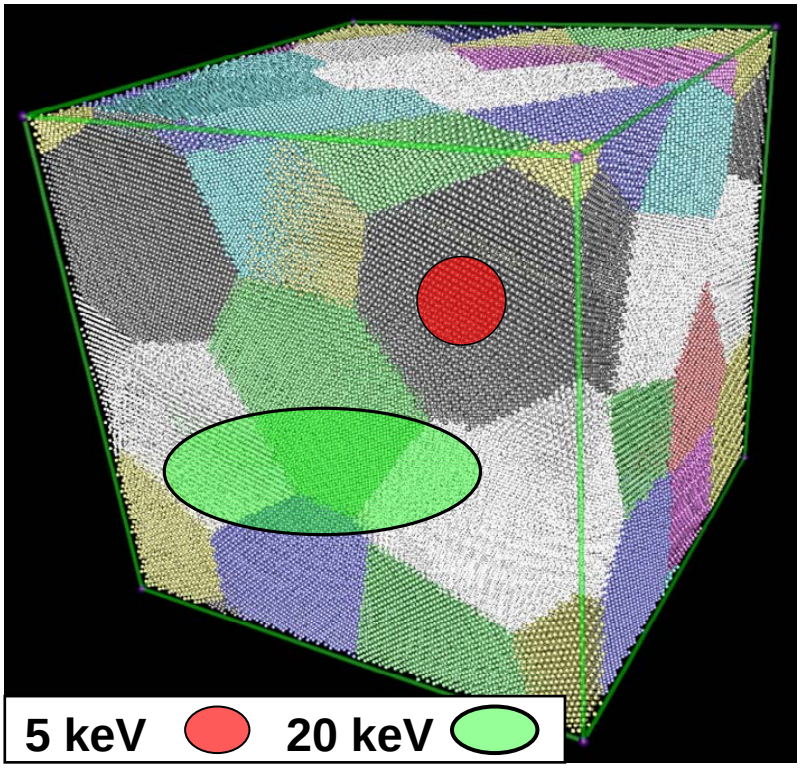

Fig. 1. MD simulation cell, 32 ~10 nm grains. Shaded red circle and green ellipse indicate approximate size of 5 and 10 keV cascades, respectively.

Analysis of nanograined material

Grain boundary atoms were distinguished from atoms in the grain interior using a coordination analysis of the 1st and 2nd nearest neighbors. Point defects were identified by comparing atom positions with the structure that existed prior to initiating the cascade simulation. Atoms displaced more than 0.3 times the iron lattice parameter from any original lattice site were flagged as interstitials, and sites with no atom within 0.3 times the lattice parameter were flagged as vacancies. Possible in-grain defects were identified as those point defects which were more than one-half a lattice parameter from the original grain boundaries. Further visual analysis was done to distinguish grain boundary reconstruction from the final, remaining in-grain defects.

The results of the cascade simulations have been evaluated using standard statistical methods. From all the simulations at each cascade energy, the mean value, the standard deviation about the mean (σ), and the standard error of the mean (ε) have been calculated. The standard

error of the mean provides a measure of how well the sample mean is expected to represent the actual mean and is calculated as $\varepsilon = \sigma/n^{0.5}$, where n is the number of simulations completed.

Results

Fig. 2 compares the final defect state of typical 10 keV cascades at 100K, with the single crystal simulation shown in (a) and the nanograin simulation shown in (b). Interstitial atoms are shown as green spheres and vacant sites as red spheres. Grain boundary atoms within 3 lattice parameters of a point defect are shown as black spheres to indicate the location of the boundaries. In this case, it is clear that the cascade crossed at least one of the

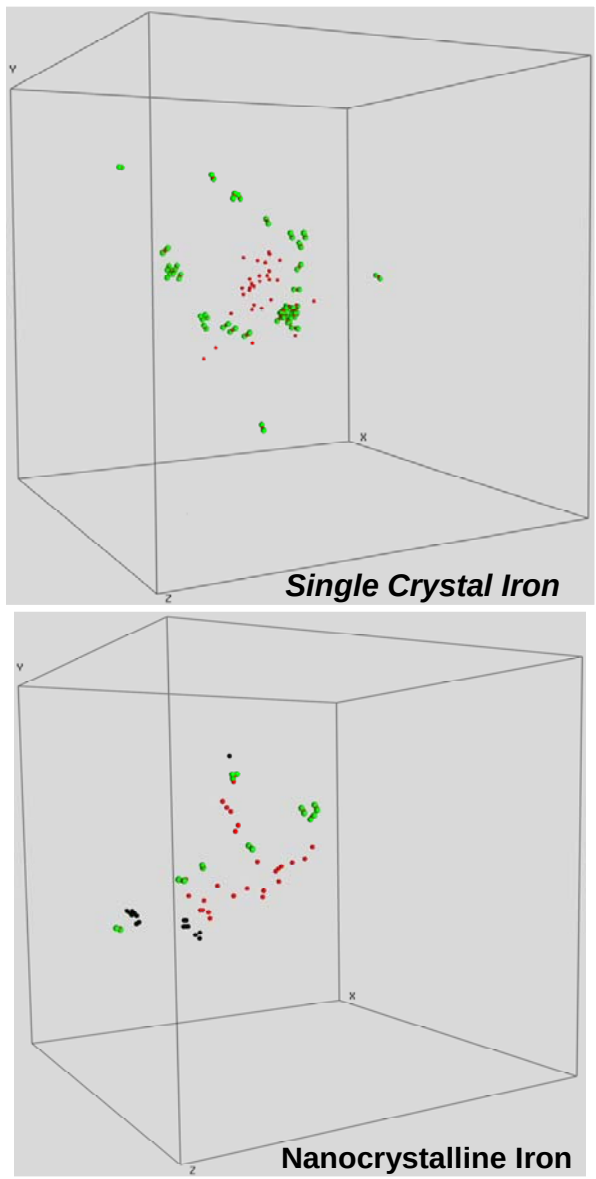

(a)

(b)

Fig. 2. Surviving point defects in 10 keV cascades at 100K for single crystal iron (a), and nanograined iron (b). Red spheres are vacant lattice sites, green spheres are atoms in interstitial positions, and black spheres are grain boundary atoms (see text).

boundaries. Even a superficial examination of these two cascades reveals dramatic differences. The total number of surviving point defects is much lower in the nanograined material, and the number of interstitial clusters is also significantly reduced. These differences are quantified in the Figs. 3 to 5.

The number of vacancies and interstitials surviving in the nanograin simulations is compared to the single crystal results in Fig. 3. A relatively wide range of cascade energies is included in Fig 3(a) to show the trend in the single crystal data, while Fig. 3(b) highlights the differences at the temperature and energy of the nanograin simulations. Mean values are indicated by the symbols in Fig. 3(a) and the height of the bars in Fig. 3(b), and the error bars indicate the standard error in both cases. The number of vacancies surviving in the nanograined material is similar to the single crystal data for 10 keV cascades, but higher at 20 keV. Much lower interstitial survival is observed in nanograined material under all conditions.

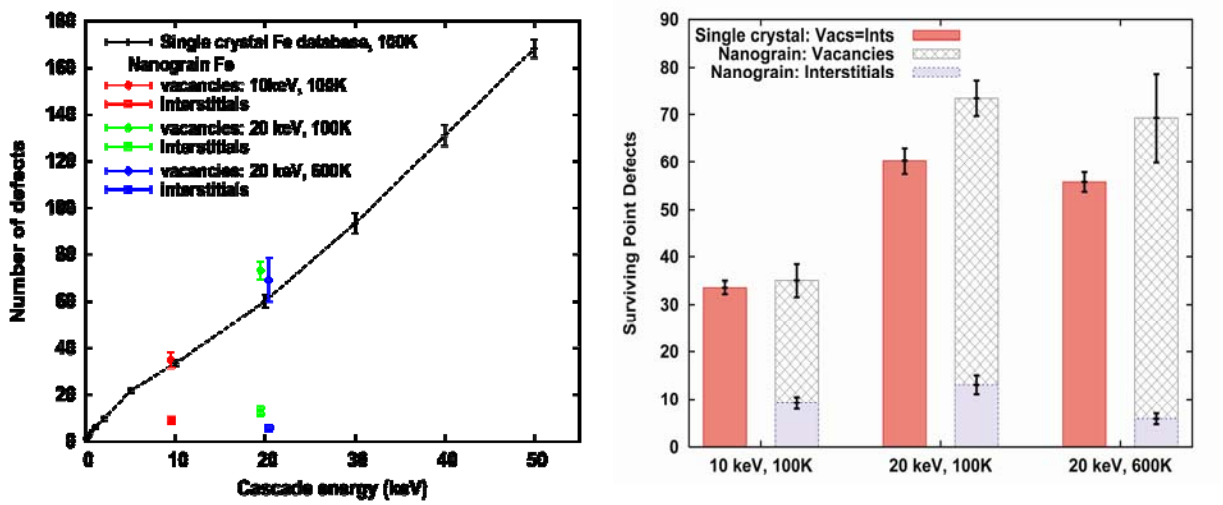

(a) **(b)**

Fig. 3. Number of stable interstitials and vacancies created by displacement cascades in single crystal and nanograined iron.

The number of surviving interstitials and vacancies that are contained in clusters is shown in Fig. 4(a) and 4(b), respectively. Consistent with the implications of Fig. 2 and the overall reduction in interstitial survival shown in Fig. 3(a), the number of interstitials in clusters is dramatically reduced in nanograined material for all the conditions examined. Compared to single crystal iron, the influence of irradiation temperature on interstitial clustering in 20 keV cascades appears to be reversed in the nanograined material. The influence of the nanocrystalline structure vacancy clustering appears to be more modest as shown in Fig. 4(b), which includes the results of only the 20 keV cascades. There is no significant change in the number of vacancies in clusters at 100K, but a statistically significant increase is observed at 600K. This again leads to a reversal in the temperature dependence of vacancy clustering between the single and nanograined iron, although the change is opposite of that observed for interstitial clustering.

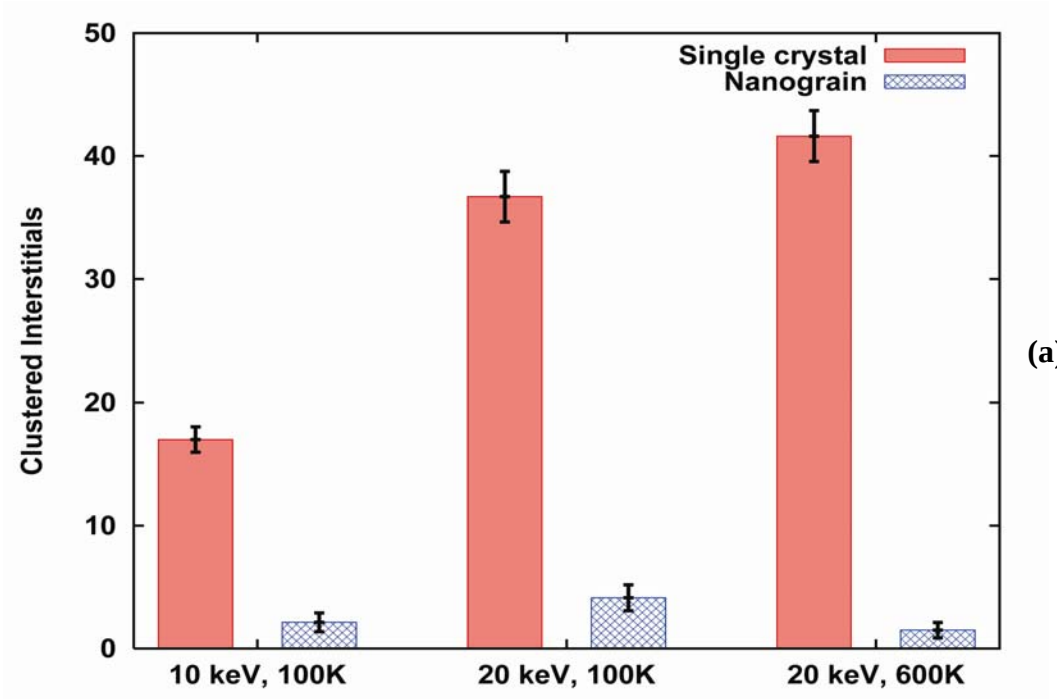

(a)

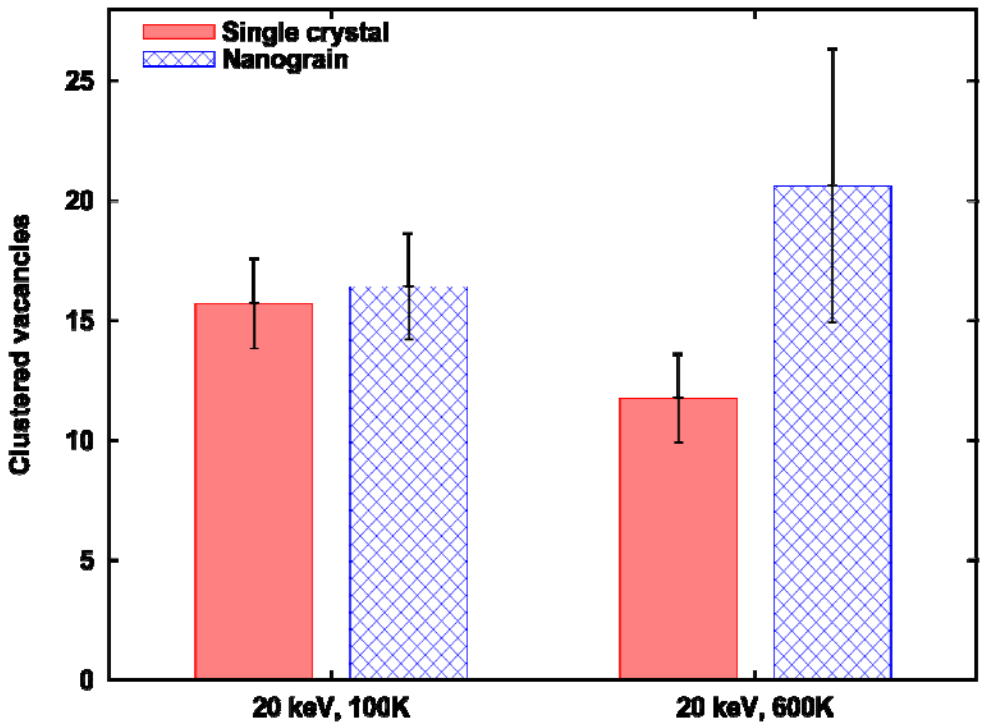

(b)

Fig. 4. Number of surviving interstitials and vacancies contained in clusters in single crystal and nanograined iron.

Since the number of surviving point defects, particularly interstitials, is so strongly reduced in the nanograin material, it is helpful to compare the fraction of defects in clusters in addition to the absolute number. Such a comparison is shown in Fig. 5 where the fractions of surviving interstitials and vacancies contained in clusters in both nanograined and single crystal iron are compared for all the conditions simulated. The changes in clustering fraction are somewhat reduced relative to the changes in the number of defects in clusters (Fig. 4), but are still substantial – particularly for interstitial defects. Notably, the reversed temperature dependence mentioned above for the number of defects in clusters in 20 keV cascades is preserved in the clustering fractions. The fraction of interstitials in clusters increases between 100 and 600K for single crystal iron but decreases for nanograined iron, while the vacancy cluster fraction decreases for single crystal iron and increases for nanograined iron.

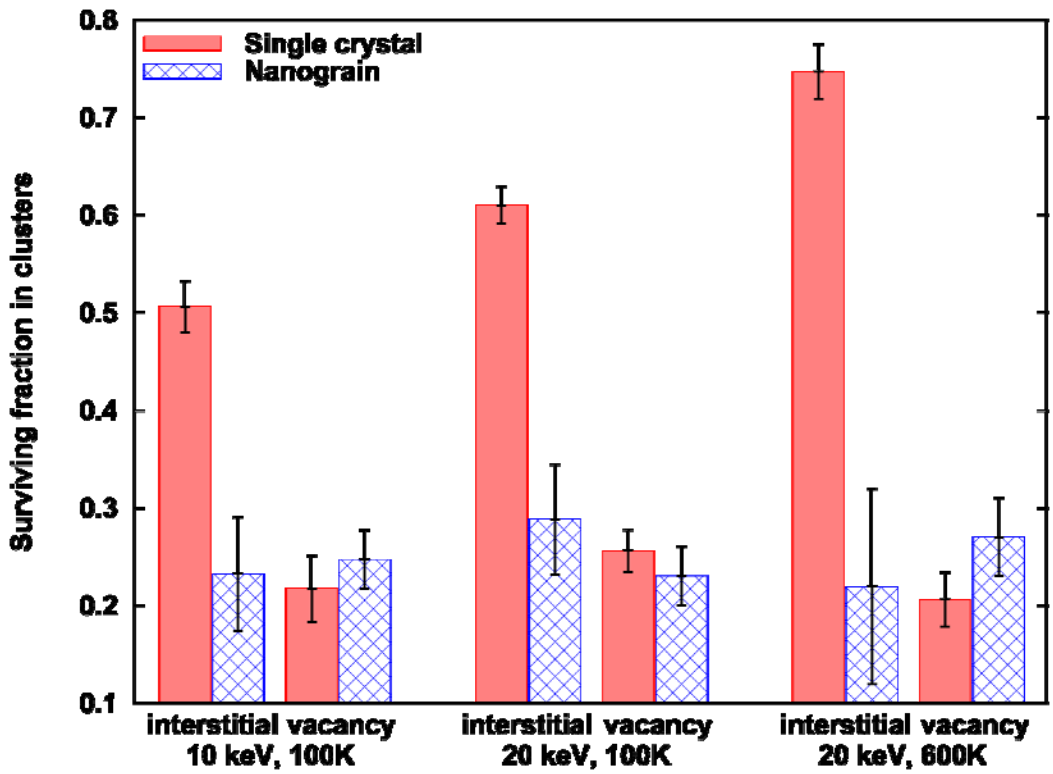

Fig. 5. Fraction of surviving interstitials and vacancies contained in clusters in single crystal and nanograined iron.

Discussion and Summary

Although the range of this study was limited in temperature and cascade energy, the results have demonstrated a strong influence of microstructural length scale (grain size) on primary radiation damage production in iron. Both the effects and the mechanisms appear to be consistent with previous work in nickel [11, 16], in which very efficient transport of interstitial

defects to the grain boundaries was observed. In both iron and nickel, this leads to an asymmetry in point defect survival. Many more vacancies than interstitials survive at the end of the cascade event in nanograined material while equal numbers of these two types of point defects survive in single grain material. The nature of the residual vacancy defect clusters is different in iron than in nickel because iron does not exhibit stable stacking faults. Similar to single crystal iron [8], few of the vacancies have collapsed into compact clusters on the MD timescale. The vacancy clusters in both single and nanograined iron tend to be loose three-dimension aggregates of vacancies bound at the first and second-nearest neighbor distances [8]. The size distribution of such vacancy clusters was not significantly different between the single and nanograin material. In contrast, the interstitial cluster size distribution was altered in the nanograined iron, with the number of large clusters substantially reduced. There appears to be both a reduction in the number of large interstitial clusters formed directly in the cascade and less coalescence of small mobile interstitial clusters since the latter are being transported to the grain boundaries.

Although the differences in primary damage formation may be significant, a more important issue is the degree to which these differences alter radiation damage accumulation over much longer times. Two factors need to be considered. The first is the difference in the nature of the surviving cluster size distributions. Having fewer large clusters could delay the formation of extended defects that lead to mechanical property changes such as hardening and embrittlement. Second, and more importantly, the fact that the number of surviving vacancies is substantially greater than the surviving interstitials is likely to bias the subsequent damage accumulation toward vacancy type defects. At times long enough for vacancy diffusion, many of the mobile vacancy defects may also be lost to the grain boundaries. Alternately, the higher vacancy supersaturation could lead to the nucleation of larger, immobile vacancy defects such as voids which could promote swelling and mechanical property changes. In order to determine whether it is the more or less benign situation that prevails, the impact of altered primary damage behavior needs to be evaluated over diffusive time scale, e.g. using mean field rate theory or Monte Carlo models [21]. The higher helium levels generated in a fusion reactor environment could influence the evolution path by stabilizing vacancy defects and preventing their transport to and absorption at grain boundaries, leading to different behavior than observed under fission neutron irradiation.

The changes in defect survival observed in these simulations are qualitatively consistent with the limited available experimental observations [13-15]. For example, Rose, et al. [13] carried out room-temperature ion irradiation experiments of Pd and ZrO_2 with grain sizes in the range of 10 to 300 nm, and observed a systematic reduction in the number of visible defects produced. Chimi, et al. [14] measured the resistivity of ion irradiated gold specimens following ion irradiation and found that resistivity changes were lower in nanograined material after room temperature irradiation. However, they observed an increased change in nanograined material following irradiation at 15K. The low temperature results could be related to the accumulation of vacancy defects as mentioned above since they should be immobile at 15K.

The results of the present study, along with the previous theoretical and experimental investigations, suggest that nanograined materials may offer a path for the development of radiation-resistant materials. The potential for reduced damage accumulation is clear, at least at higher temperatures. However, it is also clear that further work is required to develop an understanding of the mechanisms involved in order to explain observation such as the increased

resistivity change observed by Chimi, et al. [14] at 15K. The experimental results can be influenced by porosity in the sintered or compacted materials [13], and must consider the uncertainties associated with limited irradiation volumes in ion irradiations. As mentioned above, the results of MD cascade simulations provide only the starting point for a complex path of damage accumulation that must be investigated using other techniques.

Acknowledgments

Research sponsored by the Division of Materials Sciences and Engineering and the Office of Fusion Energy Sciences, U.S. Department of Energy, under contract DE-AC05-00OR22725 with UT-Battelle, LLC.

References

1. R. S. Averback, R. Benedek, and K. L. Merkle, Phys. Rev. B **18** (8), 4156 (1988).
2. A.J.E. Foreman, W.J. Phythian, C.A. English, Philos. Mag. A **66**, 571 (1992).
3. A. F. Calder and D. J. Bacon, J. Nucl. Mater. **207, 25** (1993).
4. D.J. Bacon and T. Diaz de la Rubia, J. Nucl. Mater. **216** (1994)
5. D. J. Bacon, A. F. Calder, F. Gao, V. G. Kapinos, and S. J. Wooding, Nucl. Instr. Meth. B **102**, 37 (1995).
6. W. J. Phythian, R. E. Stoller, A. J. E. Foreman, A. F. Calder, and D. J. Bacon, J. Nucl. Mater. **223**, 245 (1995).
7. R. E. Stoller, G. R. Odette, and B. D. Wirth, J. Nucl. Mater. **251**, 49 (1997).
8. R. E. Stoller, J. Nucl. Mater. **276**, 22 (2000).
9. R. E. Stoller and A. F. Calder, J. Nucl. Mater. **283-287**, 746 (2000).
10. C. S. Becquart, C. Domain, A. Legris, J.C. Van Duysen, J. Nucl. Mater. **280**, 73 (2000).
11. M. Samaras, P. M. Derlet, H. Van Swygenhoven, and M. Victoria, Phys. Rev. Lett. **88**, 125505 (2002).
12. M. W. Finnis and J. E. Sinclair, Phil. Mag. A **50**, 45 (1984) and Erratum, Phil. Mag. A **53** (1986) 161.
13. M. Rose, A. G. Balogh, and H. Hahn, Nucl. Instr. Meth. Phys. Res., Sect. B **127-128**, 119 (1997).
14. Y. Chimi, A. Iwase, N. Ishikawa, M. Kobiyama, T. Inami, and S. Okuda., J. Nucl. Mater. **297**, 355 (2001).
15. T. D. Shen, S. Feng, M. Tang, J. A. Valdez, Y. Wang and K. E. Sickafus, Appl. Phys. Lett. **90,** 263115 (2007)..
16. M. Samaras, P. M. Derlet, and H. Van Swygenhoven, Phys. Rev. B **68**, 224111 (2003).
17. M. W. Finnis, "MOLDY6-A Molecular Dynamics Program for Simulation of Pure Metals," AERE R-13182, UK AEA Harwell Laboratory (1988).
18. M. W. Finnis, P. Agnew and A. J. E. Foreman, Physical Review B **44** 567 (1991).
19. F. Gao, D. J. Bacon, P. E. J. Flewitt, and T. A. Lewis, J. Nucl. Mater. **249**, 77 (1997).
20. G. Z. Voronoi and J. Reine, Angew. Math. **134**, 199 (1908).
21. R. E. Stoller, S. I. Golubov, C. Domain, and C. S. Becquart, J. Nucl. Mater. **382,** 77 (2008).